Design and Performance Analysis of Blades Based on the Equal–Variable Circulation Method

D. Liang[1], C. Song[1], S. Liang[2], S. Wang[3], Y. Li[1] and Z. Zhou[1]*

[1]School of Electrical and Power Engineering, China University of Mining and Technology, Xuzhou, China, [2]Shandong Jirong Thermal Technology Co., Ltd., Jinan, China, [3]China National Nuclear Power Operations Management Co., Ltd., Jiaxing, China

With the aim of improving the aerodynamic performance of axial turbomachinery, a new type of blade is designed using the equal–variable circulation method. Taking an axial flow fan as the research object, this article describes the development of a new type of turbomachinery by changing the design method and producing a blade with forward sweep. The aerodynamic performance of the fan is simulated and compared with the experimental data. The numerical results show that the equal circulation design method improves the aerodynamic performance of the blade roots, while the variable circulation design method enhances the aerodynamic performance of the blade tips. By adopting the equal–variable circulation design method, the total pressure of the experimental fan is increased by about 4%, while the efficiency remains unchanged. Forward-swept blades with an equal–variable circulation design also improve performance over the conventional blades by changing the center-of-gravity stacking line. At low flow rates, the efficiency of the experimental fan can be increased by 7.5%, and the working range of the flow is expanded. Under high flow rates, the restriction of the blade tip on the airflow is decreased and the fluidity is slightly reduced.

Keywords: axial turbomachinery, equal–variable circulation method, forward sweep, aerodynamic performance, blade tip

1 INTRODUCTION

In industrial production, low-pressure axial fans are widely used because of their uncomplicated structure, large flow rates, and stable operation. In turbomachinery research, improved efficiency and reduced noise are long-standing topics of research. The modification of turbomachinery is mainly divided into three directions: airfoil modification, blade shape modification, and tip clearance modification (Peng et al., 2013; Rehman et al., 2018; Sreekanth et al., 2021).

In terms of airfoil modification, Pascu et al. (2009) and Cho et al. (2009) proposed a scheme for optimizing the blade arbitrary vortex design based on the NACA-65 series airfoil, and combined different types of design and optimization algorithms in a CFD solver to increase the blade load and efficiency. Liu et al. (Hongpeng et al., 2020) used three methods to minimize the drag coefficient, namely, affixing a zigzag trailing-edge to the trailing edge of the airfoil, using a slotted airfoil, and a combination of the zigzag method and the slotted airfoil. Sogukpinar (2018) created a new airfoil by changing the thickness of the pressure side to obtain high lift coefficient and post-stall airfoils. In general, the modification of the airfoil optimizes the aerodynamic performance.

In terms of blade shape modification, Hassan Saeed et al. (2019) modified four rotor blades and found that the new blade design performs better than other modifications. Lazari and Cattanei (2014)

optimized a non-statistical axial flow fan based on the three-parameter vortex law and the meridian runner size. By considering the aerodynamic volume and proposing its corresponding variation range, and constraining the aerodynamic design to ensure that non-statistical design parameters were used, a good aerodynamic blade was obtained. Dugao et al. (Zhou and Jiang, 1996) proposed a new type of axial fan optimization design method, and Sorensen et al. (Sørensen and Sørensen, 2000; Sørensen et al., 2000) improved this approach by using numerical methods. The application of optimization technology improves the performance of impeller machinery in terms of flow, torque, efficiency, pressure, and surge margin by changing the blade's center-of-gravity stacking line (Place and Cumpsty, 1998; Wadia et al., 1998; Gallimore et al., 2002) and the blade profile line (Burguburu et al., 2004; Chen et al., 2005; Idahosa et al., 2008). Ahn (Adjei et al., 2019) and Jang and Kim (2007) used response surface approximation to optimize the blade profile. The abovementioned studies show that the efficiency can be improved by reducing the separation zone and correcting the corner vortex.

Previous research has shown that studying the flow characteristics of forward-swept structures applied to low-speed axial fans is of certain engineering significance. However, there has been little research on the optimization of forward-swept blades for low-pressure axial fans. This article proposes a new design method of low-pressure axial flow fan, which can effectively improve the operating range and parameters of low-pressure axial flow fan for engineering practice. Moreover, studying the deep reasons for the efficiency improvement and the optimization of internal flow has practical significance for further optimization of the blade.

2 DESIGN PRINCIPLE

2.1 Design Principle of Equal–Variable Circulation

For low-pressure axial fans, the design methods can be divided into equal circulation design and variable circulation design according to the law of airflow parameters along the blade height direction. The inlet and outlet flow of the axial flow turbomachinery blades is usually designed according to the free vortex mode:

$$C_u r^\alpha = \Gamma = Const, C_z = Const, \tag{1}$$

where C_u, C_z, and r^α represent the circumferential component, axial component, and the radius of absolute velocity, respectively; Γ is the circulation. When $\alpha = 1$, the design follows the equal circulation design method; when $\alpha \neq 1$, the design comes from the variable circulation design method. The velocity triangle shows that the circumferential partial velocity C_u decreases linearly with increasing radius r.

$$\Delta p = p_2 - p_1 + \frac{1}{2}\rho\left(C_{2u}^2 + C_{2z}^2 - C_{1z}^2\right). \tag{2}$$

Here, p_1 and p_2 are the static pressure at the inlet and outlet of the impeller, respectively; C_1 and C_2 are the absolute speed at the inlet and outlet, respectively; and the subscripts u and z represent the circumferential and axial speed components, respectively. According to Euler's equation, the total pressure rise of the impeller can be expressed as

$$\Delta p = \rho u C_{2u}, \tag{3}$$

where u is the circumferential speed, which is equal to the angular velocity of the impeller ω multiplied by the radius r. Substituting Eq. 3 into Eq. 2 gives

$$p_2 = p_1 + \rho u C_{2u} - \frac{1}{2}\rho\left(C_{2u}^2 + C_{2z}^2 - C_{1z}^2\right). \tag{4}$$

Taking the derivative along the radial direction, we obtain

$$\frac{dp_2}{dr} = \frac{\rho d\left(uC_{2u}\right)}{dr} - \frac{\rho}{2}\left(\frac{dC_{2u}^2}{dr} + \frac{dC_{2z}^2}{dr}\right). \tag{5}$$

According to the radial balance equation,

$$\frac{dp_2}{dr} = \frac{\rho C_{2u}}{r}. \tag{6}$$

Substituting Eqs 6, 1 into Eq. 5 and integrating yields

$$C_{2z}^2 = 2\omega\Gamma\int dr^{1-\alpha} - \left(\frac{\Gamma}{r}\right)^2\int dr^{2-2\alpha}. \tag{7}$$

The equal circulation design method ignores the secondary radial flow and simplifies the flow of the airflow around the blade to an unmixed flow around many sections. In the variable circulation design method, the distribution of airflow parameters along the blade height does not satisfy the assumption that $C_u r = Const$. Therefore, the change in the aerodynamic parameters of the blade along the blade height is incorporated by adjusting the unequal exponent of circulation. The load factor of the blade root must be considered in the process of equal circulation design because the blade obtained through this design method has the root of the blade as its main work interval, and the load factor of other sections must be smaller than its root. Therefore, the root load factor must satisfy certain requirements. Traditionally, when the load at the root of the blade is relatively large, the variable circulation design is needed to further improve the total pressure coefficient.

During the blade design process, if the root load factor satisfies the necessary conditions, the equal circulation design and the variable circulation design can be combined to further optimize the aerodynamic shape of the blade. A blade root with a larger load factor can be designed using the equal circulation design method, while a tip with a smaller load factor can be designed with the variable circulation design method. Therefore, the equal–variable circulation design method effectively increases the chord length of each section of the blade, optimizes the aerodynamic shape of the blade, and increases the working force of the blade.
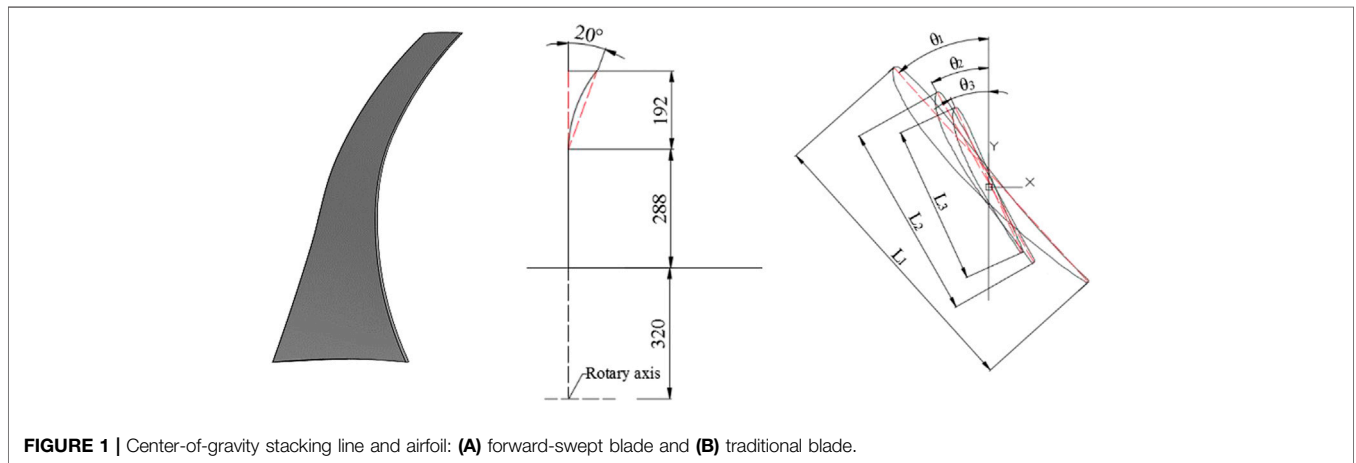
FIGURE 1 | Center-of-gravity stacking line and airfoil: **(A)** forward-swept blade and **(B)** traditional blade.

2.2 Design Principle of Forward-Swept Blades

The calculation model is constructed after the aerodynamic design calculation according to the equal–variable circulation design method. As a forward-swept blade is used in the experiments, this blade type is described in detail here. The reference airfoil for the blade design is the LS airfoil. According to the reference (Yang, 2008), the forward sweep of the blade ranges from 40 to 70% of the span, and the forward-sweep angle ranges from 10° to 20°. Three sections with different blade heights are shown in **Figure 1**. The specific parameters of the fan blade are listed in **Table 1**.

3 EXPERIMENTAL AND NUMERICAL METHODS

3.1 Experimental Methods

The experimental fan is a single-stage low-speed axial-flow fan, as is widely used for indoor ventilation in the textile industry. The experimental parameters are given in **Table 2**. The performance of axial flow fans can be tested with an experimental device. The device has a pressure sensor installed between the outlet of the collector and the inlet of the fan, and this sensor collects pressure signals and motor parameters, as shown in **Figure 2**. The hub ratio of the fan is 0.4, the rotation speed is 980–990 rpm, the outer

diameter of the fan cylinder is 1,600 mm, the length of the intake cylinder is 4,000 mm, and the measured length is 4,815 mm.

3.2 Numerical Methods

In this study, ANSYS CFX was used for numerical simulations. The calculations use a single-flow-channel model. The physical model is divided into three regions: the inlet cylinder, fan rotor, and outlet cylinder. For the inlet and outlet, ICEM was used to divide the structural grid; for the rotor part, Autogrid was used to divide the grid to ensure sufficient grid quality. The single runner grid of the rotor is shown in **Figure 3**. The boundary conditions and convergence criteria are presented in **Table 3**.

To eliminate the influence of the grid resolution on the numerical results, four sets of rotor partial grids were selected for calculation. In the grid-independence verification, the SST k – ω turbulence model was used for calculation, and the $Q_v - P_{total}$ results under different conditions were compared. As shown in **Figure 4**, as the grid resolution increases, the calculated total pressure value gradually increases. When the number of grid cells in the rotor region reaches 240,000, the upward trend is no longer obvious. This shows that the number of grid cells no longer affects the calculation results. The final number of grid cells was selected to be 240,000.

Different results can be obtained with different turbulence models, so the accuracy of the turbulence model was verified. As

TABLE 1 | Parameters of forward-swept blades.

Parameters of forward-swept blades	
θ_1	45°–58°
θ_2	17°–30°
θ_3	12°–35°
L_1	236.12 mm
L_2	135.50 mm
L_3	122.53 mm
α	0.6–1

TABLE 2 | Parameters of experimental device.

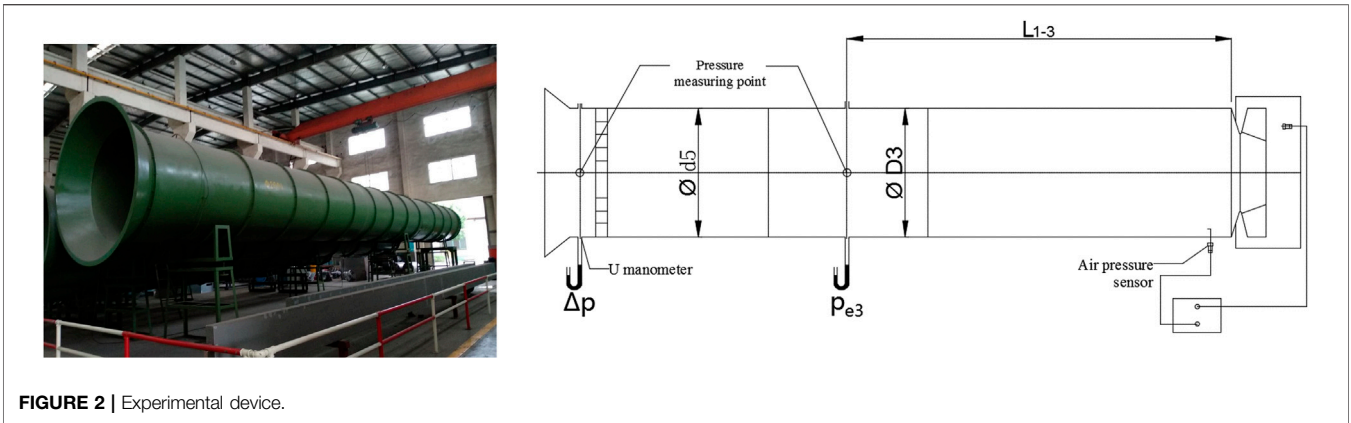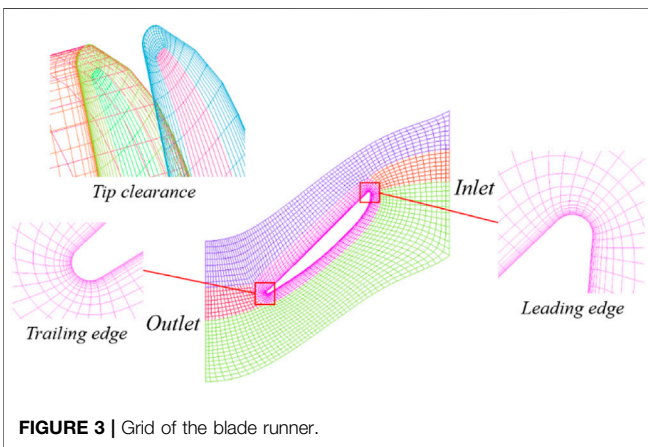| Experimental method	C-type experiment (pressure inlet and opening outlet)
Flow measurement	Conical imported nozzle
Power measurement	Electrometric method
Rotor diameter	1,600 mm
Speed	980–990 rpm
Measuring length	4,815 mm
Intake duct	4,000 mm

FIGURE 2 | Experimental device.

FIGURE 3 | Grid of the blade runner.

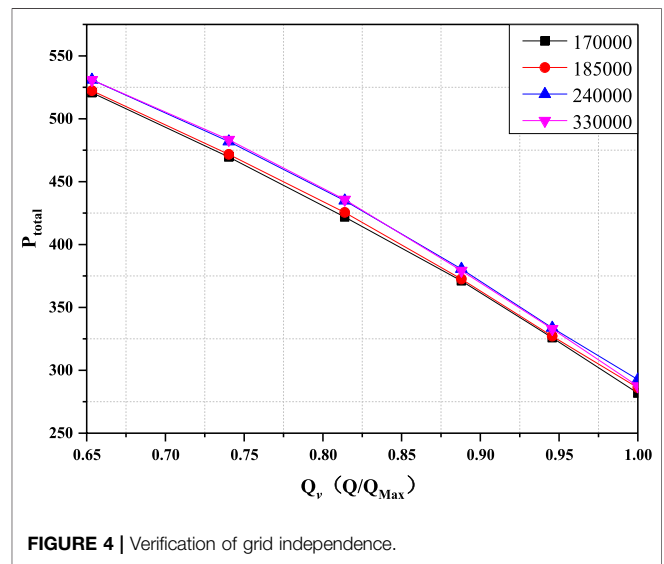FIGURE 4 | Verification of grid independence.

TABLE 3 | Boundary conditions and calculation convergence criteria.

Boundary	Value
Inlet boundary	Mass flow rate
Outlet boundary	Open boundary condition
Rotational speed	980–990 rpm
References pressure	101.325 kPa
Blade surface	No-slip wall
Turbulence models	SST $k - \omega$
Solver	Double precision
Convergence criteria	1×10^{-4}

shown in **Figure 5**, the calculated total pressure given by the SST $k - \omega$ model is closer to the experimental value than that in the standard $k - \varepsilon$ model and the RNG $k - \varepsilon$ model in all conditions. At $0.4Q_v$–$0.65Q_v$, the relative error obtained by the SST $k - \omega$ turbulence model becomes larger because the fluid flow in this region is accompanied by a large amount of flow separation and a large number of vortices are shed near the blades. At $0.65Q_v$–$1Q_v$, the existence of the blade tip clearance grid causes slight deviations between the calculated values given by the three turbulence models and the experimental data, resulting in small errors in the efficiency calculations.
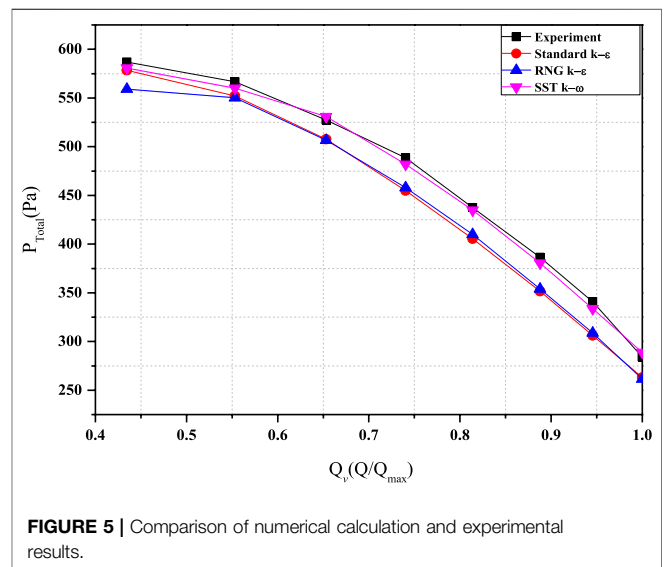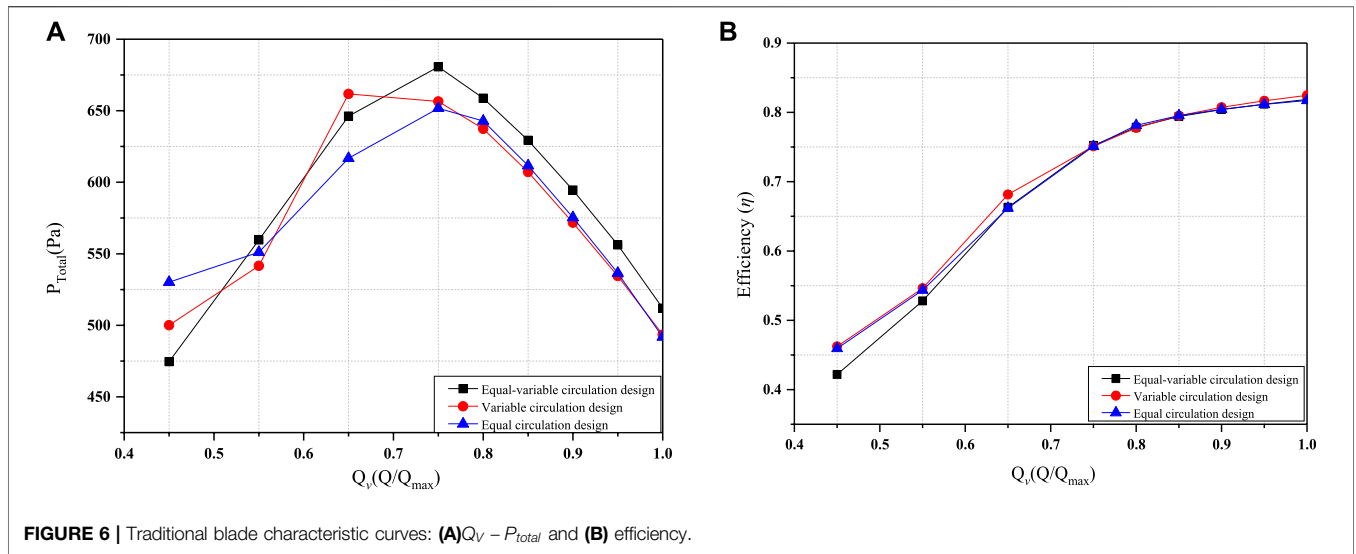

FIGURE 5 | Comparison of numerical calculation and experimental results.

FIGURE 6 | Traditional blade characteristic curves: **(A)** $Q_V - P_{total}$ and **(B)** efficiency.

The calculation results of the SST $k - \omega$ model are close to the experimental values for $0.4Q_v$–$0.65Q_v$, because the SST $k - \omega$ model uses a hybrid function to solve the transition from the standard $k - \varepsilon$ model near the wall to the high Reynolds number $k - \varepsilon$ model outside the boundary layer. In addition, the SST $k - \omega$ model uses a modified turbulence viscosity formula to solve the transport effect caused by turbulent shear stress, thus obtaining a high-precision solution for the separated flow. Therefore, even if the influence of the blade tip clearance grid is considered in the calculation, the SST $k - \omega$ model still obtains a solution that is close to the experimental value. In summary, the SST $k - \omega$ turbulence model is the most suitable for use in the scenarios considered in this article.

4 RESULTS

4.1 Conventional Blade With Equal–Variable Circulation Design

Figure 6 compares the $Q_v - P_{Total}$ curves and the $Q_v - \eta$ curves given by the equal–variable circulation design blade, the variable circulation design blade, and the equal circulation design blade at various design installation angles, $\eta = (P_{Total} \cdot Q_v / 1, 000 \cdot 3, 600)/\pi \cdot \text{torque} \cdot n \cdot 360, 000)$. As shown in **Figure 6A**, when the relative flow rate is greater than $0.7Q_v$, the total pressure of the equal–variable circulation design blade is higher than that of the equal circulation design blade and the variable circulation design blade, giving a maximum total pressure increase of 4%. At $0.65Q_v$, the total pressure of the variable circulation design blade is higher than that of the equal–variable circulation design blade. This is because the secondary radial flow is considered in the design of variable circulation blades and the effect of centrifugal force on the flow is controlled by selecting an appropriate variable circulation index. This reduces the flow separation of the hub and the formation of a low-pressure region, and

FIGURE 7 | Axial velocity comparison at the exit.
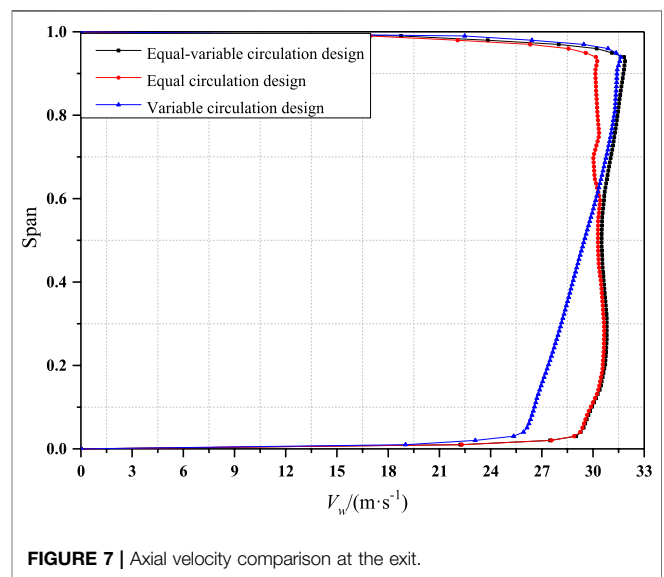
optimizes the flow in the impeller under low flow conditions. The equal–variable circulation design blade is designed to give an equal circulation quantity below 60% of the span (i.e., its main work part). This leads to the weak constraints of airflow in low flow conditions and the formation of a larger separation zone near the hub. Therefore, the total pressure of the equal–variable circulation design blade is lower than that of the variable circulation design blade at $0.65Q_v$.

It can be seen from **Figure 6B** that the efficiency of the equal–variable circulation design blade is basically the same as that of the other two blades. Thus, the equal–variable circulation design significantly increases the total pressure of the fan without affecting the efficiency.

Under rated flow conditions, the axial velocity of the fluid in the fan is an important parameter in determining the performance of the fan blade. **Figure 7** shows the

distribution of axial velocity (v_w) at the blade outlet along the blade height ($span$) of the equal–variable circulation design blade, the equal circulation design blade, and the variable circulation design blade. The relative blade height is defined as $span = (r - r_h)/r_s$, where r is the radial blade height, r_h is the hub radius, and r_s is the impeller radius. It can be seen from **Figure 7** that the axial velocity at the exit of the impeller of the variable circulation design blade is unevenly distributed and its value gradually increases along the radial blade height. This is because the influence of the variable circulation index is considered in the variable circulation design process; therefore, the chord length and installation angle of the section at the root of the blade are small, and the airflow restriction is weakened. For comparison, the axial velocity distribution of the equal circulation design blade is more uniform and its value gradually decreases from the root to the tip of the blade. At blade heights below 60% of the span, the axial velocity of the equal circulation design blade is greater than that of the variable circulation design blade. At blade heights above 60% of the span, the axial velocity of the equal circulation design blade is smaller than that of the variable circulation design blade. The axial velocity distribution of the equal–variable circulation design blade is more uniform at the exit. The axial velocity from the root to the tip of the blade is greater than both the equal circulation design blade and variable circulation design blade. Compared with the variable circulation design blade, the equal–variable circulation design blade adopts the equal circulation design method at less than 60% of the span, which increases the installation angle and the length of the chord line, twists the blades, and improves the working ability. Therefore, the flow conditions below 60% of the span are optimized, and the significant increase in axial speed further enhances the performance of this blade. Compared with the equal circulation design blade, the equal–variable circulation design significantly optimizes the axial velocity above 60% of the span. At blade heights above 60% of the span, the centrifugal force of the airflow is significant, and the influence caused by the radial velocity cannot be ignored. In contrast, the influence of radial velocity is not considered in the process of equal circulation design, so its axial velocity is lower at larger blade heights. The equal–variable circulation design method uses the variable circulation design at the top of the blade, which reduces the effect of centrifugal force on the airflow at the top of the blade and enhances the blade performance.

Figure 8 shows the axial velocity and cross-sectional streamlines of the three blades at 20 and 80% of the span. By comparing the axial velocity of the three blades at 20% of the span, it can be seen that the equal–variable circulation design blade has significantly more high-speed areas on the suction surface than the variable circulation design blade. Combined with the conclusions obtained from **Figure 7**, it can be inferred that the equal–variable circulation design blade achieves better performance when the relative leaf height is small. The axial velocity distribution of the equal–variable circulation design blade is similar to that of the equal circulation design blade,

which is also consistent with the conclusions indicated by **Figure 7**. The calculated average axial velocities of the equal–variable circulation design blade and the equal circulation design blade at 20% of the span are 30.2113 m/s and 29.8192 m/s, respectively, indicating that the equal–variable circulation design further optimizes the performance of the root of the blade. Comparing the axial speeds of the three blades at 80% of the span, the area of the high-speed region of the suction surface given by the equal–variable circulation design blade is significantly larger than that of the equal circulation design blade. The average speeds are 30.4782 m/s and 29.5967 m/s, respectively, and so the relative increase of the equal–variable circulation design blade in the tip region is 2.9% compared with the equal circulation design blade. The average axial velocity of the variable circulation design blade (30.0035 m/sat 80% of the span) is slightly lower than that of the equal–variable circulation design blade. Thus, the equal–variable circulation design not only optimizes the flow at the root of the blade but also further optimizes the flow at the tip of the blade. The equal–variable circulation design enhances the axial velocity at the blade root, thus enabling a larger volume of fluid to pass. In addition, it also increases the area of the high-speed region at the top of the blade, thus strengthening the restriction of air flow. This further improves its working ability and optimizes the overall performance of the impeller.

4.2 Effect of Blade Forward Sweep

The blade's center-of-gravity stacking line was modified on the basis of the equal–variable circulation design to obtain a forward-swept blade. In **Figure 9**, the forward-swept blade designed by the equal–variable circulation method has a wider stable working area than the traditional blade. This is because the forward-swept blade changes the blade tip profile, thus changing the inflow conditions, air flow structure, and blade load distribution in the blade tip area. These changes are conducive to the radial flow balance of the flow field and the transport of low-energy fluid at the blade tip. Under the full flow condition, the total outlet pressure and efficiency are the greatest when the initial blade height of the forward sweep is at 60% of the span. However, the blades show different characteristics under other flow conditions. The total pressure and efficiency are always maximized when the forward sweep starts at 60% of the span in forward-swept blades under full flow conditions, with an increase of up to 40 Pa and approximately 2%, respectively, compared with 50% of the span forward-swept blades. The 40 and 70% span forward-swept blades show similar aerodynamic performance, and their total pressure and efficiency are basically the same under all flow conditions. In conclusion, the starting height of the forward sweep has an effect on the aerodynamic performance of the blades. There is an optimum value that produces the best aerodynamic performance. For the fan studied in this article, the best aerodynamic performance can be obtained by starting the forward sweep at 60% of the span.

Figure 10 compares the performance curves of forward-swept blades with different sweep angles. The results show that the forward-sweep angle has an effect on the aerodynamic
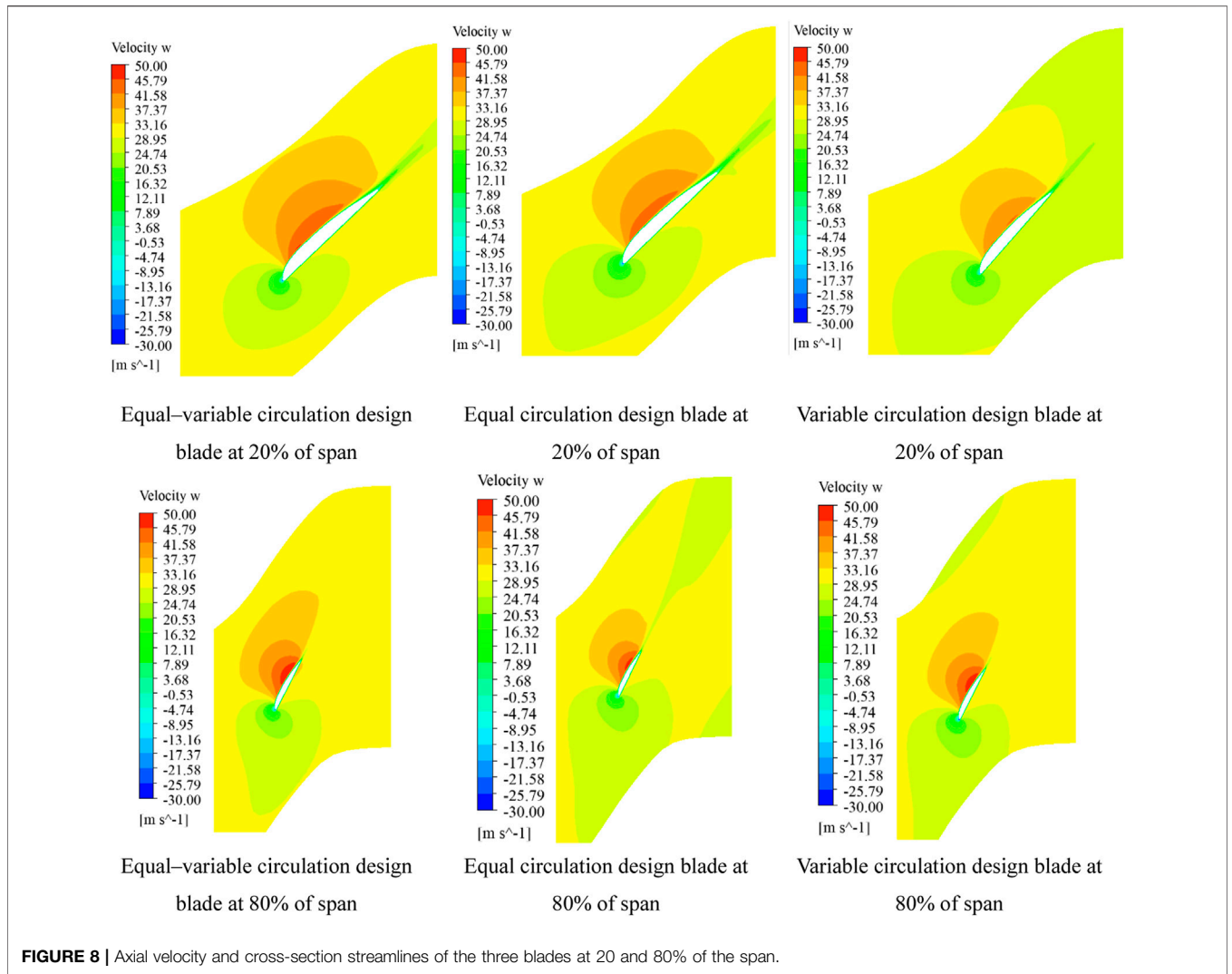
FIGURE 8 | Axial velocity and cross-section streamlines of the three blades at 20 and 80% of the span.
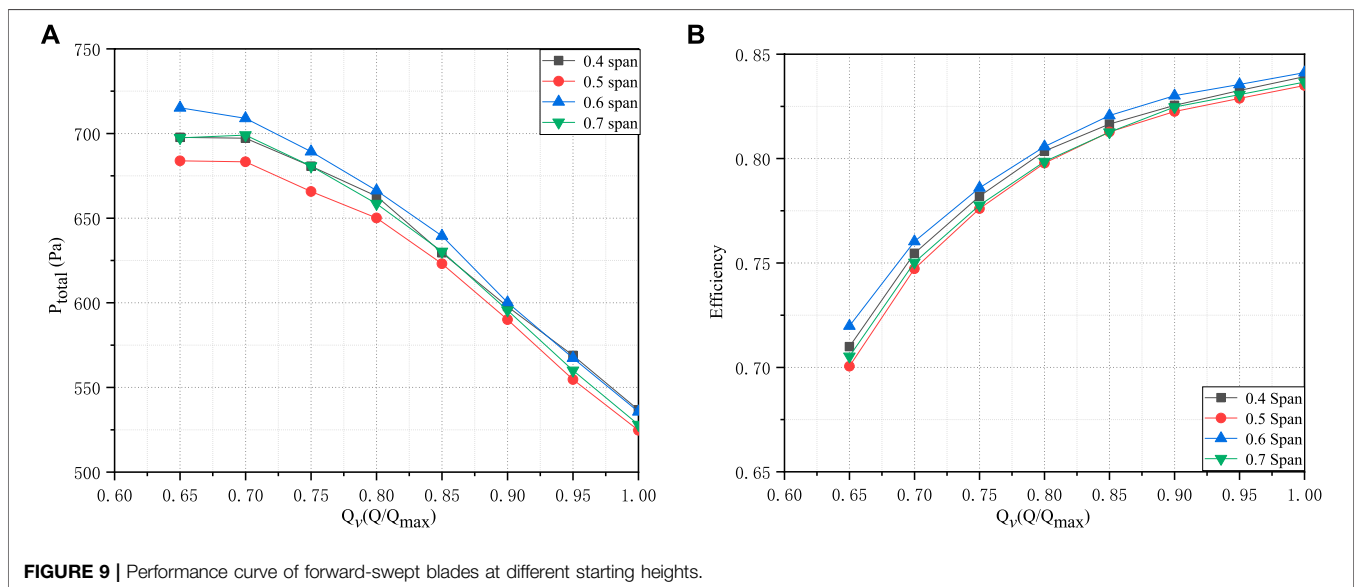

FIGURE 9 | Performance curve of forward-swept blades at different starting heights.
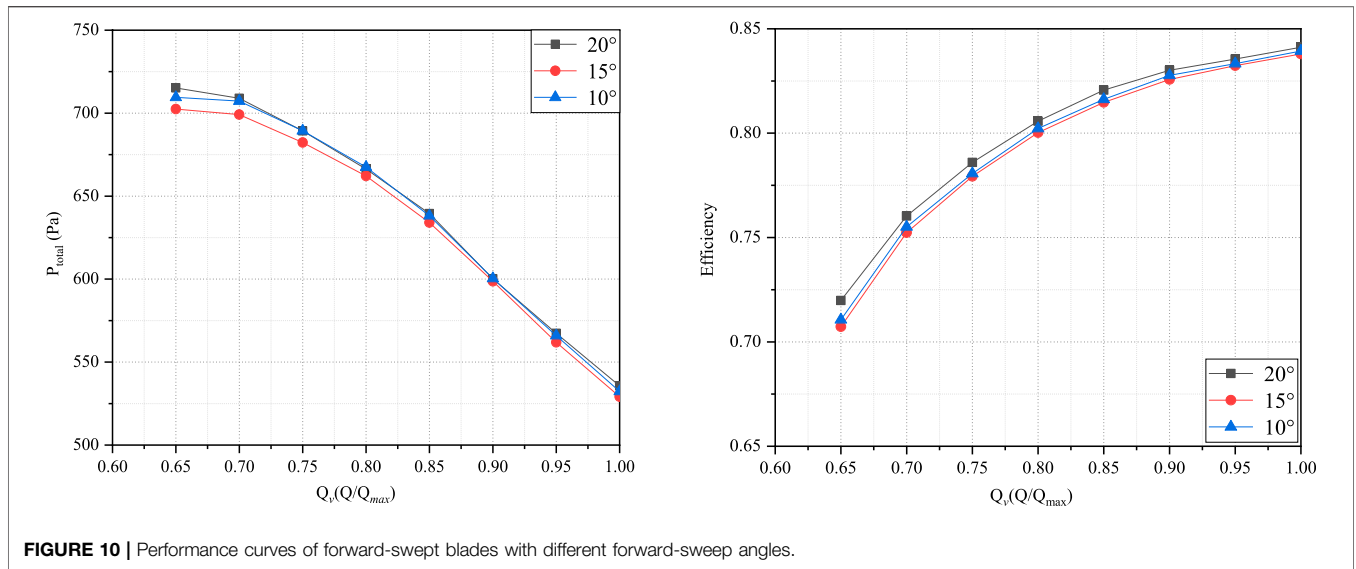
FIGURE 10 | Performance curves of forward-swept blades with different forward-sweep angles.
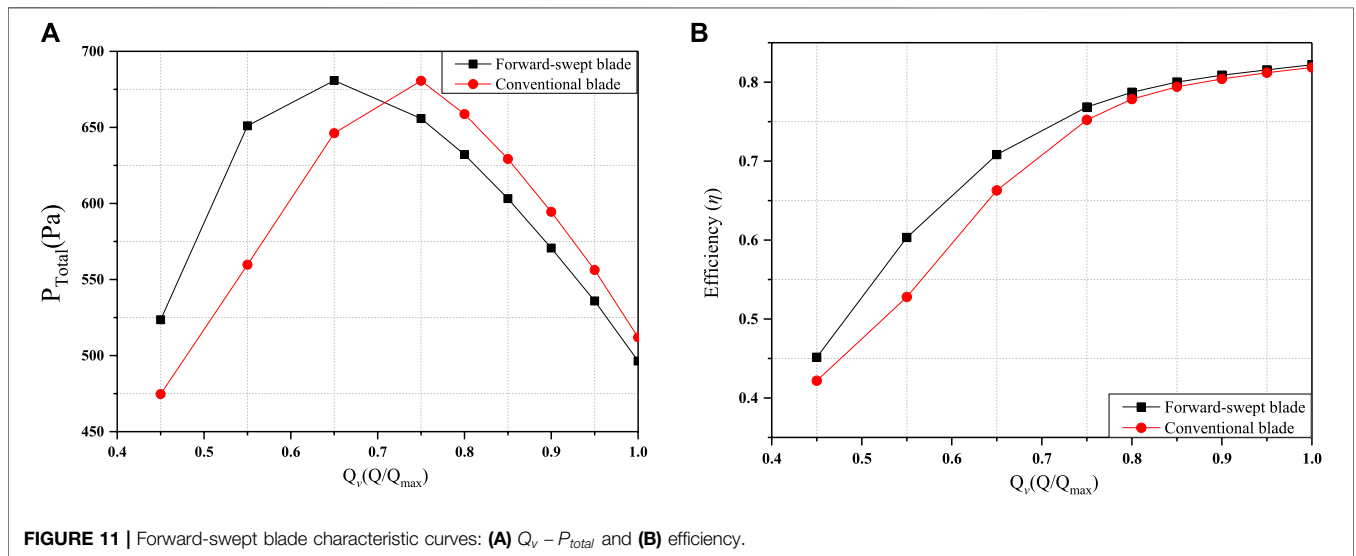

FIGURE 11 | Forward-swept blade characteristic curves: **(A)** $Q_v - P_{total}$ and **(B)** efficiency.

performance of the blade and has an optimal value. The total pressure of blades with forward sweeps of 10° and 20° is higher than that of blades with a forward sweep of 15°. In addition, blades with 20° forward sweep are slightly higher than those with 10° forward sweep at low flow conditions, creating a differential of 15 Pa. The efficiency of blades with 20° forward-sweep angle is greater than that of other blades, with an improvement of 1.5% in maximum efficiency under the full flow condition.

4.3 Aerodynamic Performance Analysis of Forward-Swept Blades With Equal–Variable Circulation Design

Figure 11 compares the aerodynamic performance of a forward-swept blade and a conventional blade. It can be seen from

Figure 11A that the conventional blade has a higher total pressure at high flow rates, indicating better aerodynamic performance. However, the forward-swept blade has a higher total pressure at low flow rates, suggesting a wider range of high pressures. **Figure 11B** shows that the forward-swept blade slightly improves the efficiency of the impeller under large-scale flows, and its efficiency is generally higher than that of the conventional blade. This is broadly similar to the conclusions obtained in the references. (Lazari and Cattanei, 2014; Zhou and Jiang, 1996; Sørensen and Sørensen, 2000; Sørensen et al., 2000). In general, the performance of the conventional blade has been greatly improved by using a forward-swept blade. In the low flow condition, the forward-swept blade improves the efficiency of the fan by 7.5%.

To further study the internal flow conditions of forward-swept and traditional blades under low flow conditions, the section flow
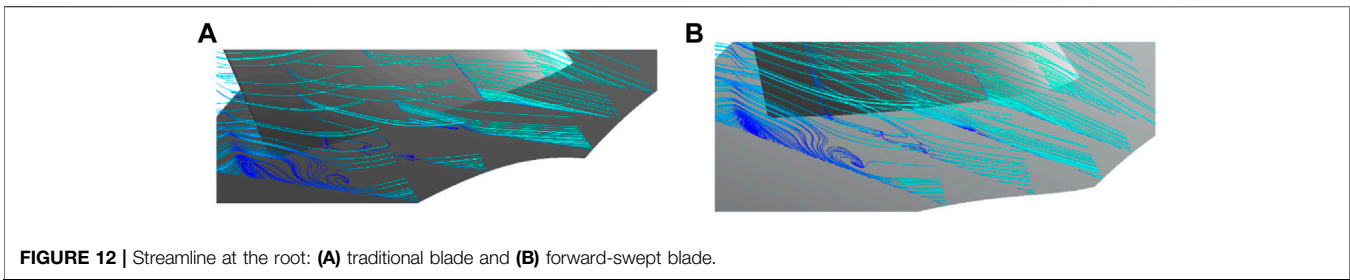
FIGURE 12 | Streamline at the root: **(A)** traditional blade and **(B)** forward-swept blade.
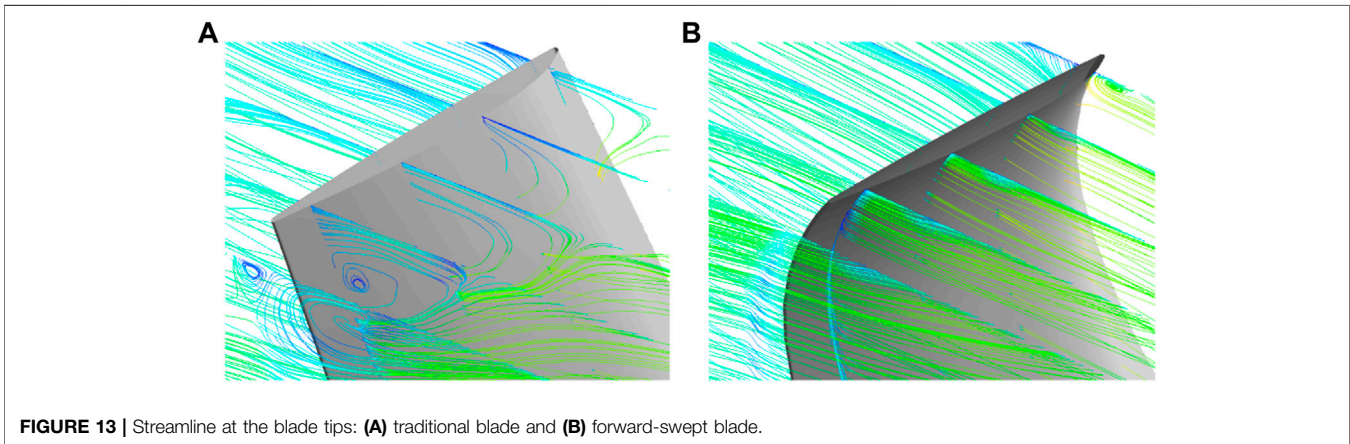

FIGURE 13 | Streamline at the blade tips: **(A)** traditional blade and **(B)** forward-swept blade.

pattern method (Liang et al., 2021) is used to observe the internal flow field of different regions, and the streamlines from five characteristic sections are selected. As shown in **Figure 12**, both traditional blades and forward-swept blades suffer corner separation at $0.65Q_v$. Comparing **Figure 12A** with **Figure 12B**, the flow characteristics at the blade root of the forward-swept blade and the traditional blade are consistent under low flow conditions.

Figure 13 shows that there are vortices at the tip of the traditional blade. As the air flow contacts the blade, a vortex forms at the tip of the blade around the front edge of the blade suction. With the gradual development of the mainstream in the channel, this vortex interacts with the wake after leaving the blade to form two vortices with opposite rotation directions. As a low-energy fluid, the rotation of the vortex itself will cause energy dissipation and affect the surrounding fluid, resulting in a decrease in the mainstream velocity at the blade tip and the deterioration of the flow state. The forward-swept blade makes the tip of the blade work on the fluid in advance, making the flow more stable. As shown in **Figure 13**, there is no wake vortex at the trailing edge, and only a small-scale vortex is formed at the leading edge. After the forward-sweep modification of the equal–variable circulation design, the flow at the blade tip under low flow conditions can be optimized. That is, the energy dissipation at the blade tip is reduced and the stable operation range of the fan is improved.

Figure 14 shows the radial distribution of the axial velocity at the exit of the impeller with the forward-swept blades and conventional blades designed by the equal–variable
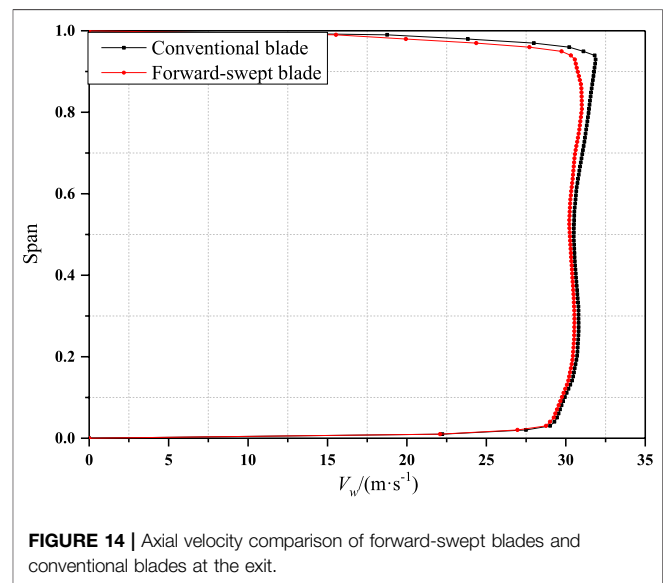

FIGURE 14 | Axial velocity comparison of forward-swept blades and conventional blades at the exit.

circulation method at $1Q_v$. As can be seen from **Figure 14**, the axial velocity distribution at the exit of the forward-swept blade at less than 60% of the span is similar to that of the conventional blade. However, the average axial velocity of the forward-swept blade at the tip of the blade is lower, which makes the mass flow of the forward-swept blade impeller (7.2475 kg/s) slightly smaller than that of the conventional blade impeller (7.37 kg/s). Although the tip of the blade adopts a variable

circulation design method, the radial constraint of the blade tip to the airflow is still weak due to the change in the blade's center-of-gravity stacking line. This results in a lower axial velocity at the tip of the forward-swept blade, and this phenomenon is especially obvious above 80% of the span. Beyond 80% of the span, the axial velocity of the forward-swept blade decreases. However, the axial velocity of the conventional blade at the blade tip is continuously increasing. This phenomenon indicates that the change of the blade's center-of-gravity stacking line may worsen the flow at the tip of the blade while increasing the efficiency and optimizing the operating range. The increase in the axial velocity between 60 and 80% of the span proves that the equal–variable circulation design can partly reduce the flow deterioration.

5 CONCLUSION

1) The equal–variable circulation design method can be applied for the design of forward-swept blades and conventional blades. The efficiency of equal–variable circulation design blades is basically the same as the blades from the equal and variable design methods, but the total pressure can be increased by 4%. The equal–variable circulation designed blades have a more stable axial velocity from the root to the tip of the blade, a greater axial velocity, and a stronger circulation capacity. The axial velocity of the equal–variable circulation designed blades is higher than that of the other two blade types. The equal–variable circulation design effectively increases the chord length of each section of the blade. Thus, combining the advantages of the equal circulation design and the variable circulation design effectively enhances the blade's performance.

2) Different forward-sweep heights will have different impacts on the aerodynamic performance of the blade. There is an optimal forward-sweep height that gives the best aerodynamic performance. In this study, a forward

sweep starting at 60% of the blade height with an angle of 20° gives the optimum efficiency.

3) The conventional blades designed by the equal–variable circulation design method achieve higher total pressures when the flow rate is larger. The forward-swept blades designed by the equal–variable circulation design method have higher efficiency and a wider stable operating area. As the flow rate decreases, the traditional blade will produce large shedding vortices at the blade tip. The forward-swept blade can effectively inhibit the formation of these vortices and improve the efficiency of turbomachinery. The change in the blade's center-of-gravity stacking line may optimize the flow at the tip of the blade while increasing the efficiency and optimizing the operating area.

DATA AVAILABILITY STATEMENT

The original contributions presented in the study are included in the article/Supplementary Material; further inquiries can be directed to the corresponding author.

AUTHOR CONTRIBUTIONS

SL, SW, YL, and ZZ provided experimental ideas and theoretical guidance. CS provided language guidance and writing guidance. All authors contributed to the article and approved the submitted version.

FUNDING

REFERENCES

Adjei, R. A., Wang, W., and Liu, Y. (2019). Aerodynamic Design Optimization of an Axial Flow Compressor Stator Using Parameterized Free-form Deformation. *J. Eng. Gas Turbines Power* 141 (10), 101015. doi:10.1115/1.4044692

Burguburu, S. p., Toussaint, C., Bonhomme, C., and Leroy, G. (2004). Numerical Optimization of Turbomachinery Bladings. *J. Turbomach.* 126 (1), 91–100. doi:10.1115/1.1645869

Chen, N. X., Zhang, H. W., Du, H., Xu, Y. J., and Huang, W. G. (2005). Effect of Maximum Camber Location on Aerodynamics Performance of Transonic Compressor Blades. *Proc. ASME Turbo Expo* 6, 1117–1125. doi:10.1115/GT2005-68541

Cho, C.-h., Cho, S.-y., and Kim, C. (2009). Development of an Axial-type Fan with an Optimization Method. *Front. Energ. Power Eng. China* 3 (4), 414–422. doi:10.1007/s11708-009-0038-5

Gallimore, S. J., Bolger, J. J., Cumpsty, N. A., Taylor, M. J., Wright, P. I., and Place, J. M. M. (2002). The Use of Sweep and Dihedral in Multistage Axial Flow Compressor Blading-Part I: University Research and Methods Development.

ASME Turbo Expo. Power Land, Sea, Air 124 (4), 521–532. doi:10.1115/1.1507333

Hassan Saeed, H. A., Nagib Elmekawy, A. M., and Kassab, S. Z. (2019). Numerical Study of Improving Savonius Turbine Power Coefficient by Various Blade Shapes. *Alexandria Eng. J.* 58 (2), 429–441. doi:10.1016/j.aej.2019.03.005

Hongpeng, L., Yu, W., Rujing, Y., Peng, X., and Qing, W. (2020). Influence of the Modification of Asymmetric Trailing-Edge Thickness on the Aerodynamic Performance of a Wind Turbine Airfoil. *Renew. Energ.* 147, 1623–1631. doi:10.1016/j.renene.2019.09.073

Idahosa, U., Golubev, V. V., and Balabanov, V. O. (2008). An Automated Optimal Design of a Fan Blade Using an Integrated CFD/MDO Computer Environment. *Eng. Appl. Comput. Fluid Mech.* 2 (2), 141–154. doi:10.1080/19942060.2008.11015217

Jang, C. M., and Kim, K. Y. (2007). Applications of Numerical Optimization Techniques to Design of Axial Compressor Blades. *J. Aerospace Power* 22 (004), 645–652. doi:10.1016/S1001-6058(07)60030-4

Lazari, A., and Cattanei, A. (2014). Design of Off-Statistics Axial-Flow Fans by Means of Vortex Law Optimization. *J. Therm. Sci.* 23 (6), 505–515. doi:10.1007/s11630-014-0735-1

Liang, D., Li, Y., Zhou, Z., Wiśniewski, P., and Dykas, S. (2021). Structure and Topology Analysis of Separated Vortex in Forward-Swept Blade. *Front. Energ. Res.* 9, 693596. doi:10.3389/fenrg.2021.693596

Pascu, M., Miclea, M., Epple, P., Delgado, A., and Durst, F. (2009). Analytical and Numerical Investigation of the Optimum Pressure Distribution along a Low-Pressure Axial Fan Blade. *Proc. Inst. Mech. Eng. C: J. Mech. Eng. Sci. 1989-1996 (vols 203-210)* 223 (C3), 643–657. doi:10.1243/09544062JMES1023

Peng, K., Fan, D., Yang, F., Fu, Q., and Li, Y. (2013). Active Generalized Predictive Control of Turbine Tip Clearance for Aero-Engines. *Chin. J. Aeronautics* 26 (5), 1147–1155. doi:10.1016/j.cja.2013.07.005

Place, J. M. M., and Cumpsty, N. A. (1998). Discussion: "Comparison of Sweep and Dihedral Effects on Compressor Cascade Performance" (Sasaki, T., and Breugelmans, F., 1998, ASME J. Turbomach., 120, Pp. 454-463). *J. Turbomach.* 120 (3), 463–464. doi:10.1115/1.2841739

Rehman, S., Alhems, L., and Rafique, M. (2018). Horizontal Axis Wind Turbine Blade Design Methodologies for Efficiency Enhancement-A Review. *Energies* 11 (3), 506. doi:10.3390/en11030506

Sogukpinar, H. (2018). The Effects of NACA 0012 Airfoil Modification on Aerodynamic Performance Improvement and Obtaining High Lift Coefficient and post-stall Airfoil. *Turkish Phys. Soc. 33rd Int. Phys. Congress (Tps33)* 1935, 020001. doi:10.1063/1.5025955

Sørensen, D. N., and Sørensen, J. N. (2000). Toward Improved Rotor-Only Axial Fans-Part I: A Numerically Efficient Aerodynamic Model for Arbitrary Vortex Flow. *J. Fluids Eng.* 122 (2), 318–323. doi:10.1115/1.483275

Sørensen, D. N., Thompson, M. C., and Sørensen, J. N. (2000). Toward Improved Rotor-Only Axial Fans-Part II: Design Optimization for Maximum Efficiency. *J. Fluids Eng.* 122 (2), 324–329. doi:10.1115/1.483260

Sreekanth, M., Sivakumar, R., Sai Santosh Pavan Kumar, M., Karunamurthy, K., Shyam Kumar, M., and Harish, R. (2021). Regenerative Flow Pumps, Blowers and Compressors - A Review. *Proc. Inst. Mech. Eng. A: J. Power Energ.*, 095765092110181. doi:10.1177/09576509211018118

Wadia, A. R., Szucs, P. N., and Crall, D. W. (1998). Inner Workings of Aerodynamic Sweep. *J. Turbomach.* 120 (4), 671–682. doi:10.1115/1.2841776

Yang, D. U. (2008). Internal Flow Mechanism and Experimental Research of Low Pressure Axial Fan with Forward-Skewed Blades. *J. Hydrodynamics, Ser. B* 20 (3), 299–305. doi:10.1016/S1001-6058(08)60061-X

Zhou, D., and Jiang, Z. (1996). Optimization Design of an Axial-Flow Fan Used for Mining Local-Ventilation. *Comput. Ind. Eng.* 31 (3-4), 691–696. doi:10.1016/S0360-8352(96)00229-X